applied sciences

MDPI

Communication

Controlled Creation of Contact Cracks in Additive Manufactured Components

Daniel Preston [1], Ahmed Ashour [1], Julian Wright [1,*], James Watts [1], Daniel Sanmartin [1] and Jacques Wood [2]

[1] Theta Technologies Limited, Exeter EX5 2FN, UK; dan.preston@thetandt.com (D.P.); ahmed.ashour@thetandt.com (A.A.); james.watts@thetandt.com (J.W.); daniel.sanmartin@thetandt.com (D.S.)
[2] Plymouth Science Park, Plymouth PL6 8BX, UK; jwood@plymouthsciencepark.com
* Correspondence: julian.wright@thetandt.com; Tel.: +44-(0)1392-247912

Featured Application: Creation of statistically significant reference sample sets for validation, optimization, and demonstration of non-destructive testing techniques, particularly for the additive manufacturing sector.

Abstract: Techniques for the controlled seeding and growth of cracks are urgently required for non-destructive testing technique evaluation, particularly for additive manufactured (AM) samples. This paper describes a method that uses a combination of the tensile load and the resonance excitation of notched AM samples, with in situ monitoring of the resonance frequency serving to track the crack dimensions. Mechanical low-cycle fatigue cracks, ranging in length from ~0.3 mm to ~5 mm, were successfully created in five AM samples using this technique. The samples were non-destructively characterized using optical microscopy and Nonlinear Resonance (NLR) testing. The exploitation of resonance enabled the concentration of a significant number of stress cycles on the samples in much shorter timespans than conventional fatigue testing, enabling a high throughput while utilizing compact components. Furthermore, the tracking of the resonance frequency shift throughout the process enabled non-invasive and no-contact real-time condition monitoring.

Keywords: non-destructive testing; cracks; contact cracks; resonance; flaw seeding; nonlinear; nonlinear resonance; reference samples

check for updates

Citation: Preston, D.; Ashour, A.; Wright, J.; Watts, J.; Sanmartin, D.; Wood, J. Controlled Creation of Contact Cracks in Additive Manufactured Components. *Appl. Sci.* **2023**, *13*, 11990. https://doi.org/10.3390/app132111990

Academic Editor: José António Correia

Received: 2 October 2023
Revised: 26 October 2023
Accepted: 27 October 2023
Published: 2 November 2023

Copyright: © 2023 by the authors. Licensee MDPI, Basel, Switzerland. This article is an open access article distributed under the terms and conditions of the Creative Commons Attribution (CC BY) license (https://creativecommons.org/licenses/by/4.0/).

1. Introduction

The aerospace and automotive sectors are two sectors that are beginning to integrate additive manufacturing (AM) into the production of critical components. In contrast to conventional manufacturing methods, AM offers the benefits of having low material waste and the ability to create highly optimized designs in a single stage [1]. However, these parts come with a unique range of defects and flaws which, combined with complex designs, presents challenges for the majority of conventional non-destructive testing (NDT) techniques.

Therefore, with this shifting manufacturing paradigm comes a need for rapid and cost-effective NDT techniques at scale for AM components. This is compounded by the acknowledged general need for the creation of suitable NDT reference samples [2] for technique validation, optimization, and demonstration. In order to develop and certify these techniques, reference sample sets must be produced in statistically relevant quantities with controlled representative flaws. Flaw seeding in AM parts commonly focuses on creating delaminations, pores, or holes of an idealized geometry [3]. Flaws are achieved via non-optimal build parameters (such as the scanning speed or temperature), through machining, or by inclusion in the original model file. Thermal cracks can be produced, albeit without dimensional control, via variation in the constraints of the part during cooling, or the use of low-weldability alloys [2].

Outside of additive manufacturing, a common method of seeding flaws is by the use of a fatigue or creep-fatigue apparatus. Low-cycle, notched specimen fatigue is common, due to the controlled location of initiation as well as the requirement of relatively fewer cycles until failure. Notches such as those created using electrical discharge machining are commonly used as crack initiation sites [4]. Fatigue tests may monitor the material failure with extensometers or systems of strain gauges, but, in general, monitoring for the control of crack sizes is a challenge.

To that end, Yan et al. [5] measured the propagation of a crack by means of current monitoring over its area. This relies on the fact that the voltage measured over a crack relates to the area of material in the cross section. They concluded that there is a strong correlation between the predicted crack growth from current measurements and the observed dimensions of propagation after sectioning. Richards et al. [6] explored the use of compliance measurements during conventional four-point fatigue cycling, successfully deriving a relationship between sample compliance and fatigue crack length.

An alternative method of seeding cracks is through thermal fatigue, whereby a sample is thermally cycled in a specific region using an induction coil placed on an accessible sample surface. Kemppainen et al. [7] discussed such a technique, indicating a relationship between thermal cycling parameters and surface-breaking crack propagation. However, thermal fatigue cracks are known to be morphologically different from mechanical fatigue cracks in that there are more cracks at the surface and microbranching along the crack length or at the tip [8]. This renders this technique less suitable when the user wishes to study mechanical failure in parts.

In previous work by Preston et al. [9], controlled cracks were embedded in ASTM F519 type 1A1 tensile coupons using a combination of dynamic and static loading, achieved via resonance excitation and mass-loading with steel weights ("bobs"), respectively. This enabled the material to be locally fatigued very quickly, whilst retaining control over the propagation. This is in contrast to conventional fatigue cycling, where the requisite large applied forces limit the cycling frequency to the order of 10 Hz. The in situ monitoring of crack growth was achieved by tracking the shift in the resonance frequency of the assembly. That work demonstrated that cracks of controlled dimensions could be created in conventional metal components. This paper describes the further development of the technique for the controlled generation of contact cracks in AM test coupons. A "contact crack" is defined as a flaw where the surfaces are extremely close—in partial or direct contact—without bonding in one dimension, having an aspect ratio of the length and/or width to the opening of several orders of magnitude. At various stages throughout the crack propagation process, the samples were characterized using Nonlinear Resonance (NLR) testing and optical microscopy.

2. Materials and Methods

2.1. Sample Set Description

Six test coupons were additively manufactured using 316 L stainless steel (Renishaw SS 316L-0407, Komenda, Slovenia) via laser powder bed fusion (Renishaw AM400). The samples were labelled RD120 to RD125, and were nominally identical. V-shaped notches were included in the original parts to act as crack initiation sites. The geometry and dimensions of the samples are shown in Figure 1. Mounting fixtures were included in the design so that the assembly could be constructed in a reproducible manner. Figure 2 shows the samples on the build plate, with each having the same orientation with respect to the build direction.

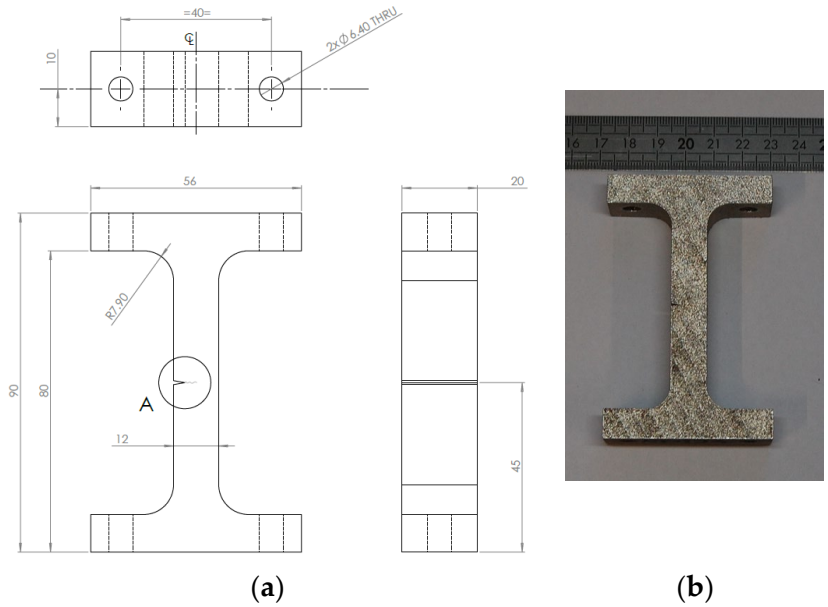


Figure 1. (**a**) Engineering drawing of each sample. The circled area labelled "A" indicates the V-notch. (**b**) Photograph of as-built sample.

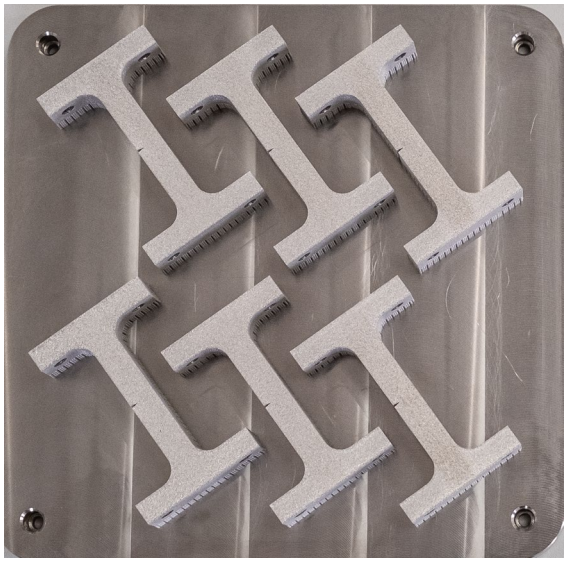


Figure 2. Samples had a common orientation on the build plate.

2.2. Experimental Setup

The flaw-induction equipment consisted of weighted samples attached to a suspension system and a large permanent magnet shaker (B&K LDS V406, Virum, Denmark). The 2.35 kg cylindrical steel bobs were required to apply a static tensile load to the sample and to reduce the resonance frequency to within the range of the system. Such a reduced frequency also exhibited higher displacements and strains, and, therefore, stresses. This is illustrated by the nomogram in Figure 3, which shows the approximate change in the frequency and displacement achieved by adding the steel bobs to the sample. The reduction in frequency was approximately one order of magnitude, while the displacement increased by approximately 260%.

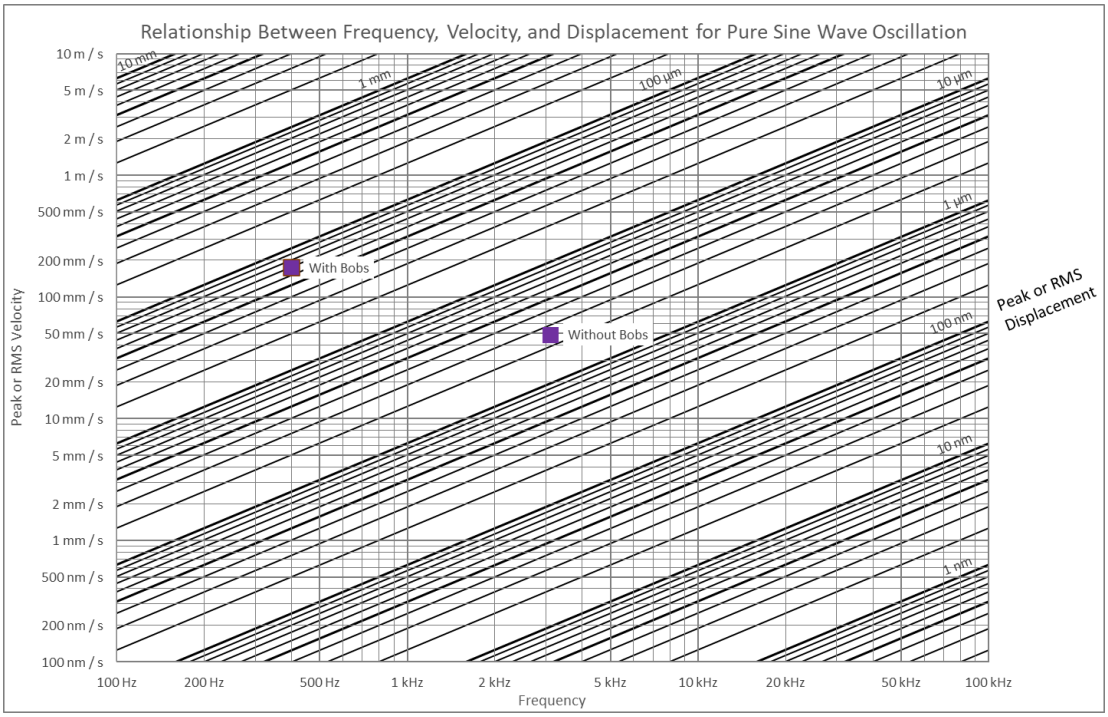
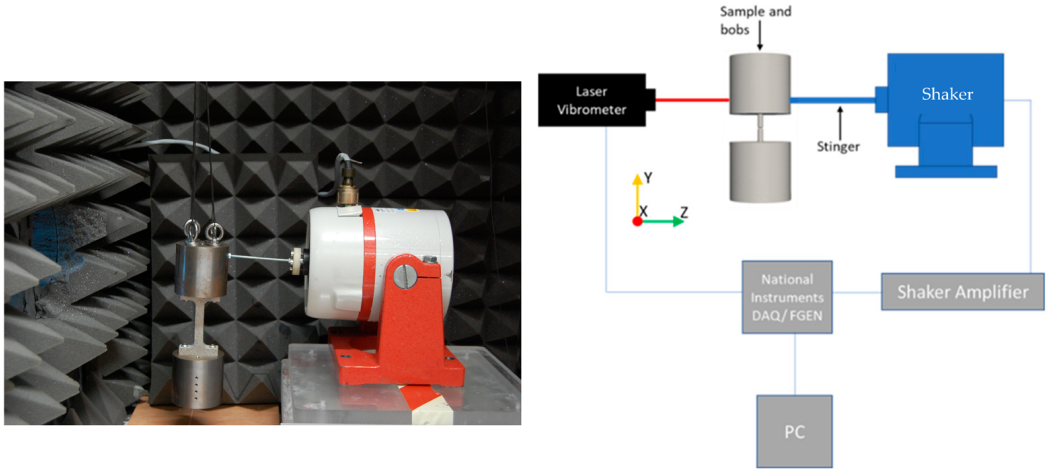


Figure 3. Nomogram to show the relationship between frequency, velocity, and displacement for the sample with and without the addition of the steel bobs.

The bobs were attached to the sample using four M6 button-head bolts, at a torque of 9 Nm. The shaker was connected to the top bob using a threaded stainless-steel rod. Laser Doppler vibrometer (LDV) measurements were taken using a Polytec PDV-100 at a point 51 mm from the top surface of the assembly, and were used to monitor the resonance frequency of the system. The initial measured velocity at this point was approximately 160 mm/s. However, because this technique utilizes whole-body resonance, no-contact measurements can be taken at any point on the assembly. A photograph and a schematic of the setup are shown in Figure 4.



(**a**) (**b**)

Figure 4. (**a**) Photograph of flaw induction system. An LDV is present off-camera, to the left-hand side of the image. (**b**) Schematic diagram of full setup, after [9].

The purpose of the system is to excite the first flexural resonance mode of the assembly at a sufficiently high amplitude so as to trigger propagation-controlled low-cycle fatigue

cracking. Obtaining a precise in situ measurement of the resonance frequency during the exposure process allows for the monitoring of crack propagation over the course of exposure, and thus, enables the controlled creation of said cracks.

2.3. Finite-Element Modelling

A finite element model was constructed using the CalculiX finite element solver version 1.0.0 to predict the resonance frequencies and mode shapes, with ParaView version 5.10.0 for the visualization of the modes. The model was computed for the samples with the two bobs bolted on the top and bottom (see Figure 5). The model was used as a guide for the vibration profile and the approximate frequency of each resonance mode. The actual excitation frequency was determined experimentally, not using the model.

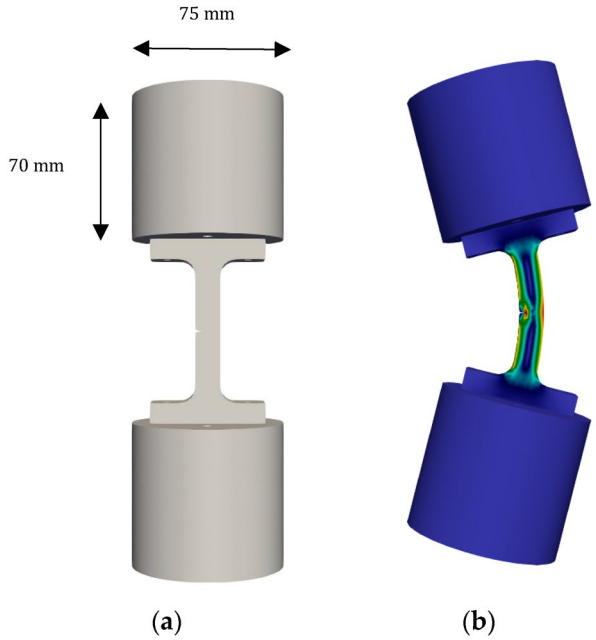


Figure 5. (**a**) CAD model of sample with bobs attached. (**b**) Mode shape of first flexural mode, with the color plot showing von Mises stress. Note that the absolute values of stress depended on the deflection amplitude.

The first flexural mode was the mode of interest for two reasons. Firstly, it concentrates stress in the desired region of the sample, at the tip of the notch. Secondly, being the fundamental mode, it has the highest displacement, making it suitable for an accelerated flaw induction process. The resonance frequency was predicted to be at 398 Hz for the sample–bob assembly.

2.4. Flaw-Induction Process and Characterization

The resonance mode was sine-swept using the shaker (±10 Hz) for 20 s. A fast Fourier transform (FFT) of the system response, as measured with the LDV, was used to determine the reducing frequency of the resonance as the crack propagated. This frequency was subsequently used as a new center of the next sine-sweep, and the process was repeated. This setup is thus capable of tracking the variation in the resonance frequency with increasing extents of induced damage. The frequency shift, Δf, is thus defined as:

$$\Delta f = f_0 - f \tag{1}$$

where f_0 is the resonance frequency of the pristine sample and f is the resonance frequency of the sample at any particular point along the flaw induction process. This Δf is taken

in this work to be a proxy for the extent of induced damage. Unless otherwise stated, the voltage supplied to the shaker was kept constant throughout the exposure process.

To evaluate the fracture point, sample RD120 was taken to complete failure, which was observed at $\Delta f_{crit} = 298.6$ Hz. To account for any potential variations in the initial conditions of the samples, a 20% safety margin was imposed on the maximum shift, Δf_{max}, induced upon the remaining samples ($\Delta f_{max} = 0.8\Delta f_{crit} = 238.88$ Hz). The samples were thus subjected to the frequency shifts shown in Table 1.

Table 1. Samples tested and their damage increments (Δf).

Sample Name	Δf Increments
RD121	$0.2\Delta f_{max}, 0.4\Delta f_{max}, 0.6\Delta f_{max}, 0.8\Delta f_{max}, \Delta f_{max}$
RD122	$0.2\Delta f_{max}, 0.4\Delta f_{max}, 0.6\Delta f_{max}, 0.8\Delta f_{max}, \Delta f_{max}$
RD123	$0.2\Delta f_{max}, 0.4\Delta f_{max}, 0.6\Delta f_{max}, 0.8\Delta f_{max}, \Delta f_{max}$
RD124	$0.2\Delta f_{max}$
RD125	$0.2\Delta f_{max}, 0.4\Delta f_{max}$

After each damage increment, each sample was removed from the flaw-induction system, detached from the bobs, and tested using NLR (Theta Technologies RD1-TT [10]). In addition, the samples were imaged using optical microscopy (Cainda digital microscope [11]) and the crack dimensions were determined using the ImageJ imaging software (version 1.53e) [12], as defined in Figure 6.

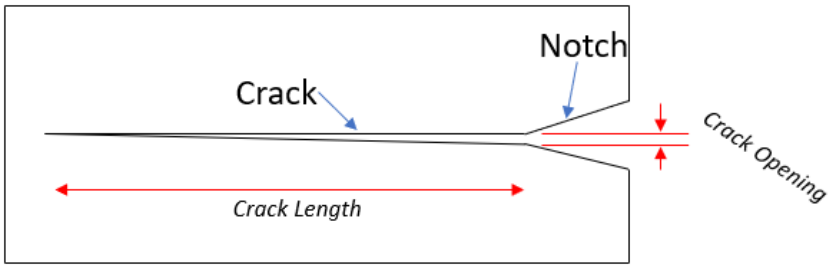


Figure 6. Schematic labelling of the crack dimensions of interest in this study.

NLR testing is an NDT technique that excites components into resonance and measures nonlinear mechanisms associated with crack-like flaws [13]. Nonlinearity can be observed in strain-dependent measurements, such as harmonic distortion or relative changes in resonance frequency [14] (in this work, referred to as "resonance drift").

Samples RD121 and RD123 were subjected to identical treatments, to assess the capability of reproducibly seeding controlled cracks of different sizes. To assess the reliability of Δf as an indicator for crack dimensions, as well as the propagation-controlled nature of this process, sample RD122 was subjected to a higher stress step, whereby, for the first damage increment, the shaker was driven at twice the voltage as the other samples. Samples RD124 and RD125 were subjected to fewer damage increments, in order to demonstrate the technique's capability to produce different crack sizes.

3. Results

3.1. Exposure Process

For sample RD120, the crack travelled through the entire thickness of the sample, causing it to break in two, as shown in Figure 7b,c. Note the very high crack tortuosity on the surface of the side opposite the notch (Figure 7b). An examination of the crack plane in Figure 7a revealed two distinct regions separated by a linear boundary: a lower-roughness large region, and a higher-roughness smaller region. The regions corresponded to two distinct failure mechanisms, with the former corresponding to the slow advance of the resonance-induced fatigue crack and the latter corresponding to the dominant fast

ductile tearing of the final section of the sample [15]. Figure 7 shows that, in spite of the surface roughness, the fracture plane indicates a macroscopically straight and flat crack morphology ahead of the notch.

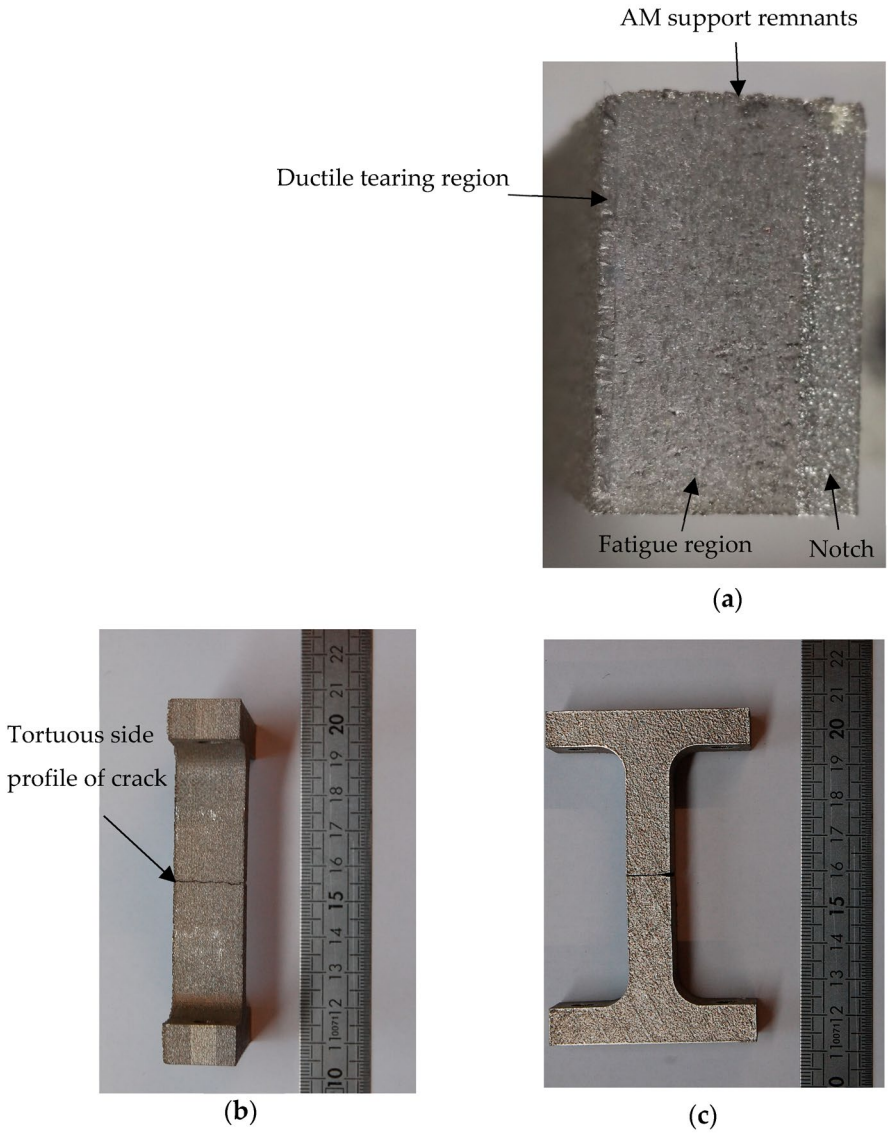


Figure 7. (**a**) Fracture surface showing two distinct failure mechanisms. The surface at the top of the image is where the sample was bonded to its AM support structure, hence the increased roughness. (**b**) RD120 side surface after complete failure, with the two halves placed together for illustrative purposes. (**c**) RD120 front surface after complete failure. Note the higher tortuosity in the side surface compared to the front surface.

During the exposure process, the resonance parameters of the system were monitored in order to track the crack propagation. Figure 8 shows the evolution of the resonance frequency of each sample plotted against the number of sweeps performed. It is this measurement that allowed for the controlled stopping of the process at different crack propagation extents. The increasing gradient over the course of the exposure indicates an increasing crack growth rate. Note the initially accelerated rate for RD122 for the first stage, followed by a curve parallel to the remaining samples. Furthermore, Figure 9 shows the resonance peak amplitude in the frequency domain, plotted against the resonance frequency for samples RD121 through RD125 throughout the exposure process. In this

work, the longest cracks generated (RD121, RD122, and RD123) took approximately 15 min in the flaw induction system.

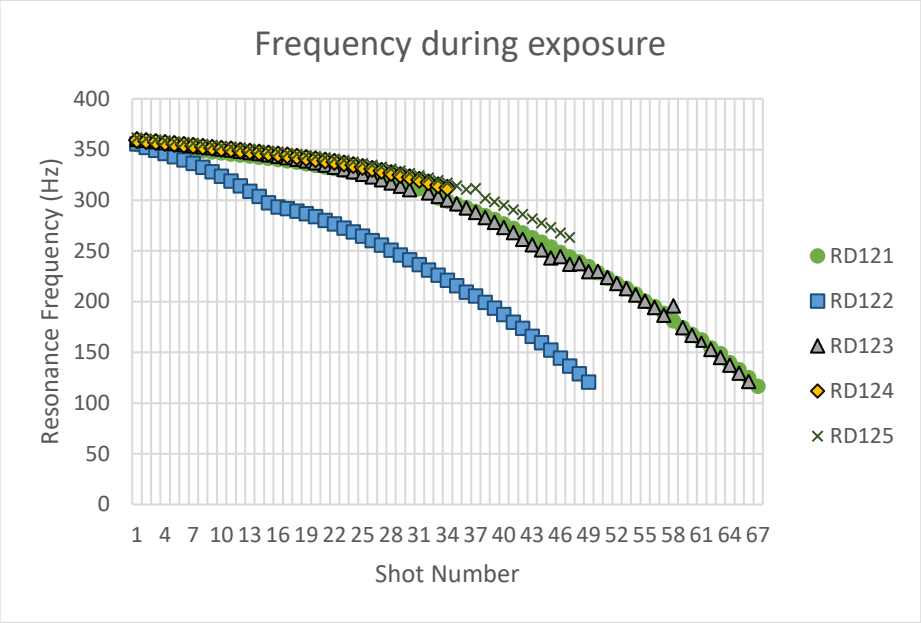


Figure 8. Evolution of resonance frequency against sweep number during exposure.

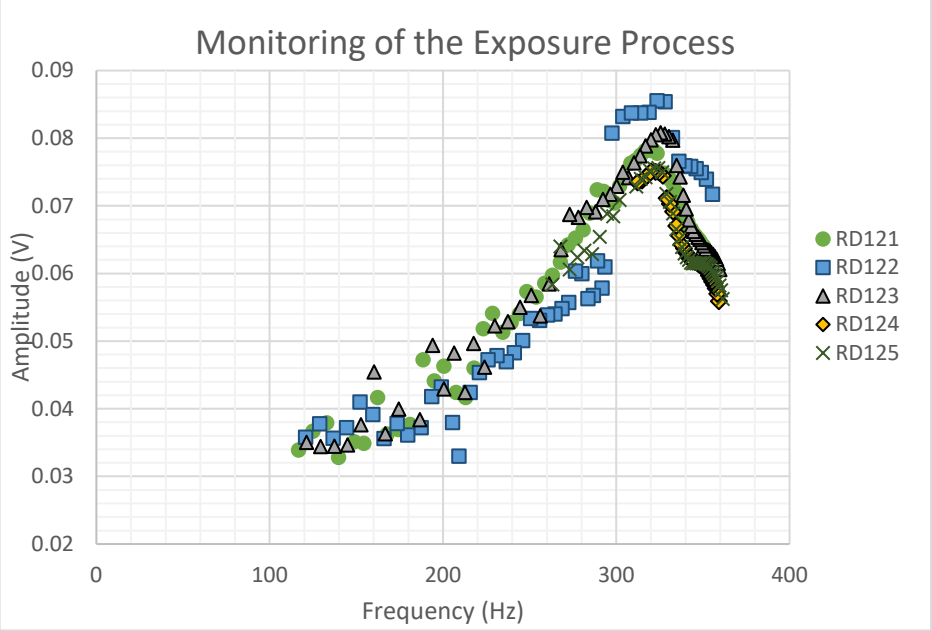


Figure 9. Evolution of resonance frequency and amplitude during exposure. Each point corresponds to a measurement from a single sine-sweep. Data from all performed sine-sweeps are presented.

The shape of the resonance peaks also changed over the course of the exposure process, as demonstrated by Figure 10. The swept peak became increasingly less symmetrical, and the transition away from the point of maximum amplitude became increasingly abrupt.

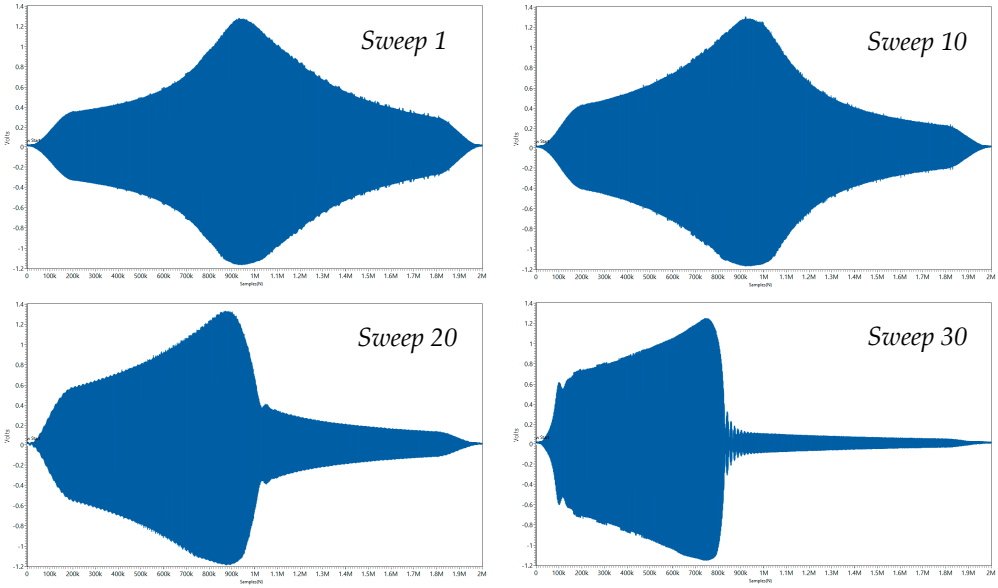
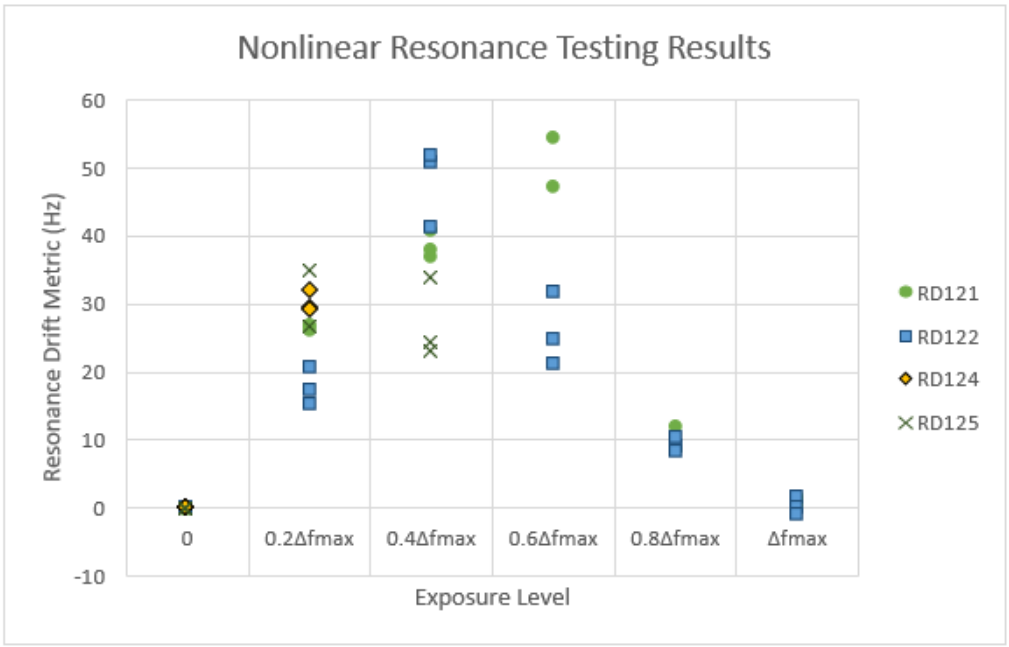


Figure 10. Time-domain waveforms showing the evolution of sample response through the exposure process.

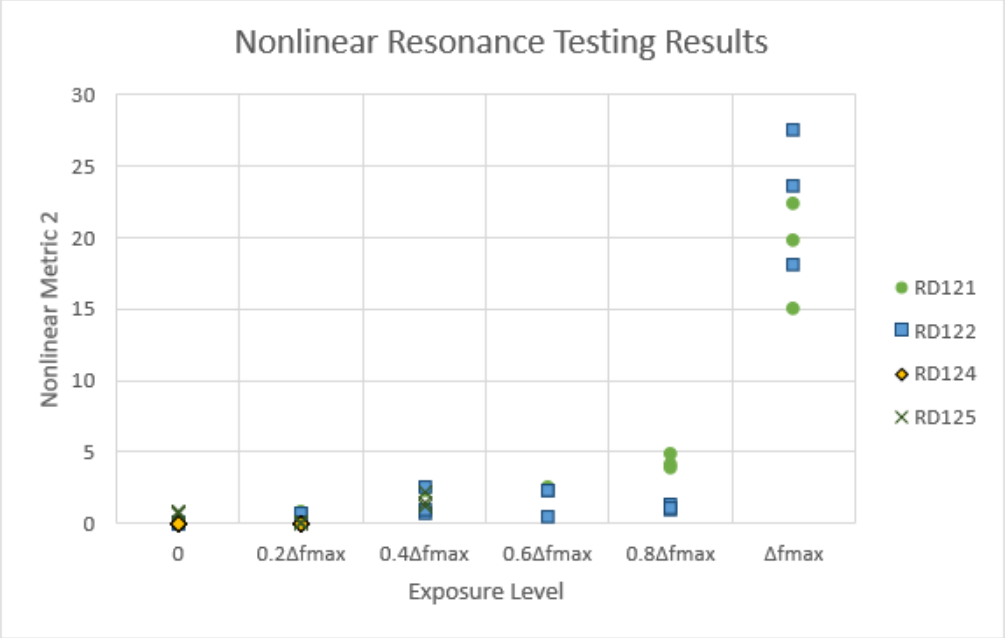
3.2. Nonlinear Resonance Results

In order to maximize the data from the small sample selection available, Nonlinear Resonance (NLR) characterization was carried out between each stage, tracking the evolution of the crack alongside the exposure. Figure 11 shows the NLR results over three separate measurements on each sample, to ensure reproducibility. Sample RD123 was omitted from the figure, as its measurements were taken at different RD1-TT settings, and were thus not comparable.



(a)

Figure 11. *Cont.*



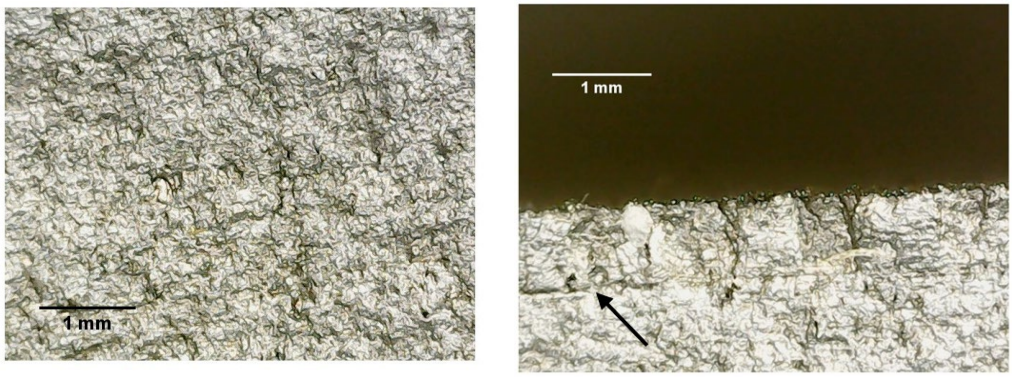
(**b**)

Figure 11. Nonlinear resonance testing results gathered between every characterization stage in order to track changes in the samples. (**a**) Resonance drift metric and (**b**) Nonlinear Metric 2. Three separate measurements were taken for each of the samples to assess the reproducibility of the measurement.

The results show that the samples in their "as-printed" states exhibited negligible frequency drift. The drift subsequently experienced a rapid rise with the damage stage, before peaking near the second/third stage and dropping off as the crack became too large. Nonlinear Metric 2, a proprietary algorithm subject to a pending patent application, showed a measured increase for the initial stages of damage, before rising sharply at the final stage.

3.3. Optical Microscopy

An optical micrograph of the fracture plane of sample RD120 is shown in Figure 12. Note the clear presence of a boundary between two regions of different roughness, indicated with an arrow.



(**a**) (**b**)

Figure 12. (**a**) Micrograph of the center of the fatigue fracture surface of RD120, showing a tortuous topography. (**b**) Distinct boundary between the fatigue and ductile fracture regions, marked by an arrow.

Because the crack plane extended across the entire sample width, the propagation could be observed using optical microscopy on the front face of the remaining samples. Figure 13 shows the microscope images of the final states of the samples.

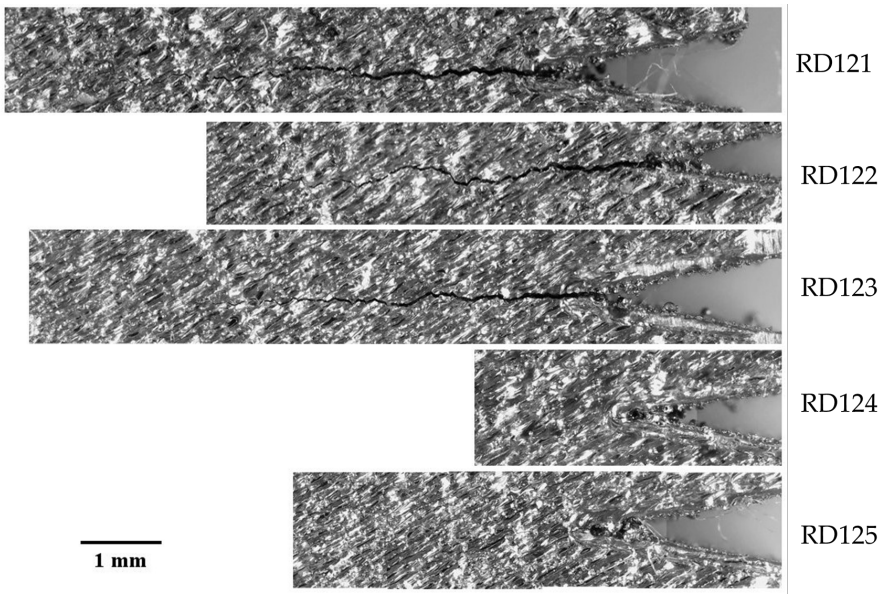


Figure 13. Microscopy images of the exposed samples, showing cracks propagating inward from the notch.

Samples RD121-123 had large cracks propagating away from the notch region. Sample RD125 had a smaller crack and sample RD124 had a very small crack that was difficult to see without polishing and, potentially, scanning electron microscopy. A magnified view of RD124 is shown in Figure 14, with red arrows indicating the crack location.

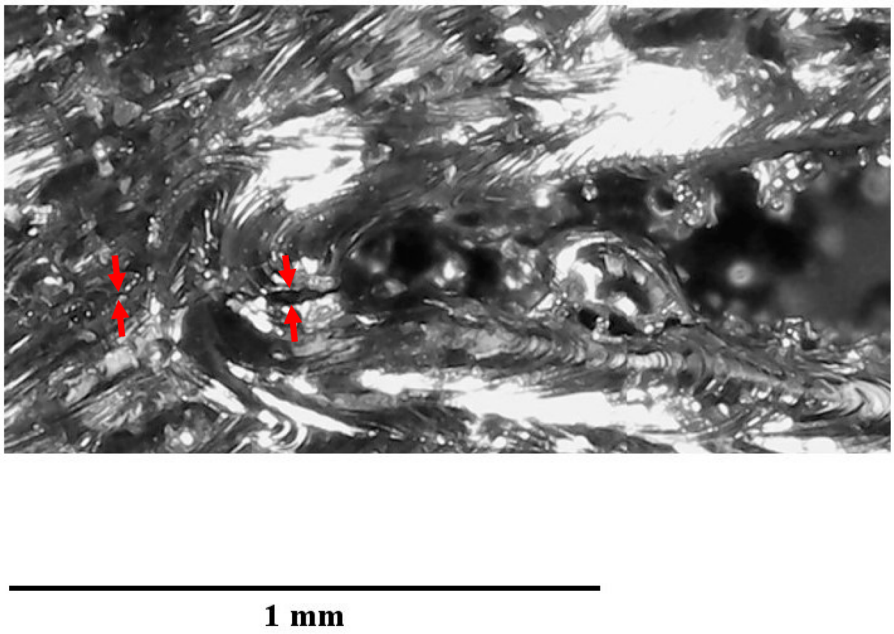


Figure 14. Magnified view of sample RD124; the red arrows highlight a very small crack present at the tip of the notch.

Crack propagation could be observed using microscopy between each of the exposure stages. Figure 15 shows a crack increasing in length over the increasing exposure levels.

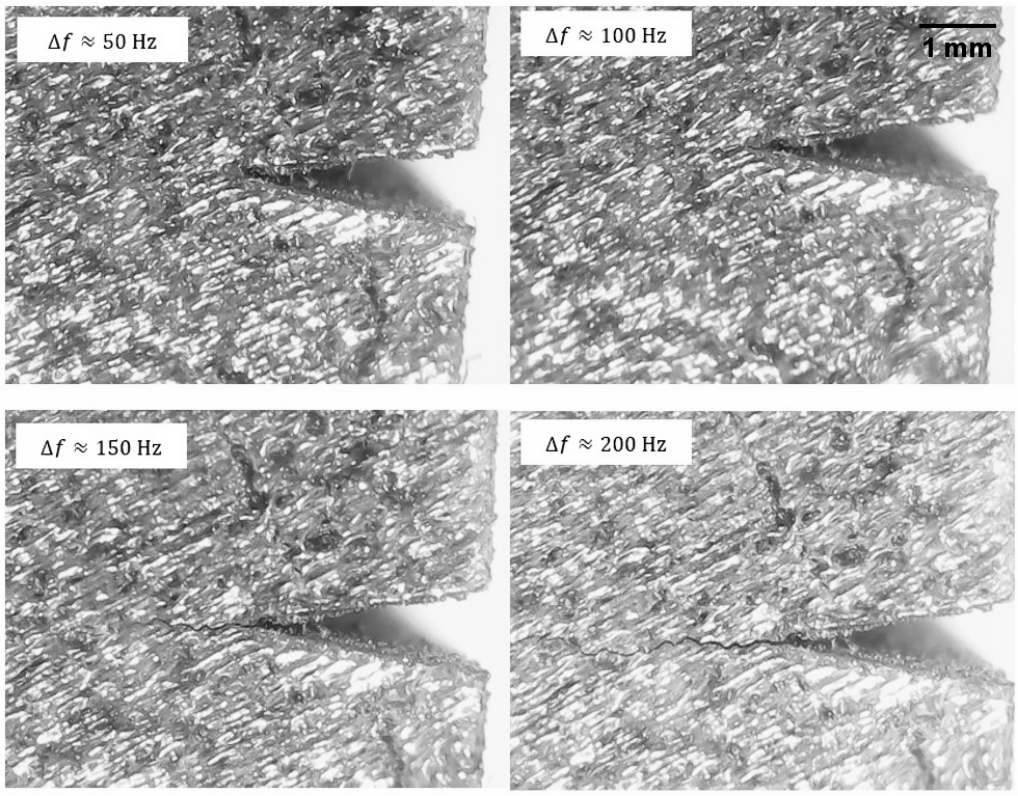


Figure 15. Micrographs of the front surface of RD122, showing the crack length progression with Δf.

From the microscopy and using the ImageJ image measurement software, approximate crack lengths and openings were obtained for the final states of the samples. Table 2 shows the length measurements of the cracks as well as the crack-opening measurements at the initiation point of the crack. Figure 16 shows the relationship between the measured crack lengths and the frequency shift (Δf) during the exposure process.

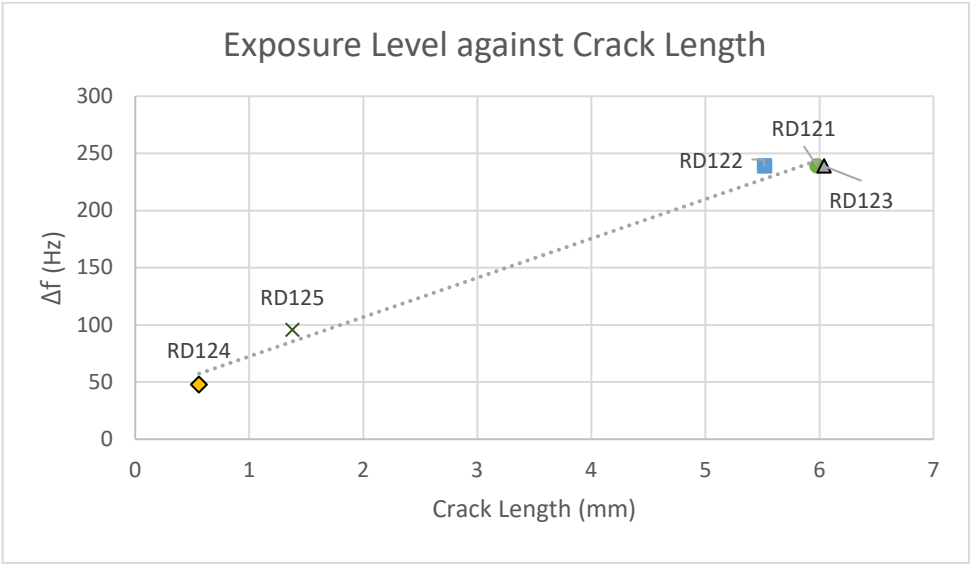


Figure 16. Frequency shift against crack length during the exposure process.

Table 2. Approximate crack dimensions, as measured from microscopy images.

Sample ID	Crack Length (mm)	Crack Opening at Initiation Site (mm)
RD121	5.98	0.079
RD122	5.52	0.077
RD123	6.04	0.063
RD124	0.56	0.014
RD125	1.38	0.015

4. Discussion

The textured topography of the fatigue region indicated an inter-granular fracture. The macroscopically flat planar nature of the fracture surface at 90° to the sample faces indicated a condition of plane strain [16]. We also noted that this crack propagated perpendicular to the build layers.

The results shown in Figures 8 and 9 indicate that the samples followed a consistent trend, in amplitude and frequency, over the course of the exposure process. As the cracks propagated, the effective stiffness of each sample decreased, causing a monotonic reduction in the resonance frequency of the sample–bob assembly. This was confirmed by Nenadic et al. [17], who demonstrated using modelling that the resonance frequency of a cracked gear tooth decreases with crack growth.

We note that the samples exhibited an immediate reduction in their resonance frequency, unlike in the previous work performed on ASTM coupons using this technique. For the latter, the resonance frequency was constant for the majority of the exposure, before a steep reduction in the frequency leading up to failure. This corroborates the propagation-controlled nature of this fatigue process. The difference is likely due to the sharp notches and rough surface features in the AM samples being efficient stress concentrators, thus acting as pre-existing flaws. Finally, we hypothesize that the spread between different samples in Figures 8 and 9 may be, in part, due to the uneven residual stress characteristic of the additive manufacturing process, as detailed in [18]. The increasing crack growth rate inferred from Figure 9 is a consequence of the receding load-bearing cross section of the samples, increasing the stress concentration ahead of the crack tip.

The samples all exhibited an initial increase in their resonance amplitude, followed by a subsequent decrease. This initial increase may be attributed to the reduced stiffness in the cracked samples. The subsequent decrease may be explained by the increasing crack growth rate towards the end of the process: eventually, during a single sweep, the crack grew by a sufficient amount to shift the resonance of the assembly away from the sweep range. This resulted in less time spent on resonance during a sweep, which manifested as an abrupt drop in the amplitude in the time-domain waveform partway through a sweep, as shown in Figure 10. Since an FFT measures the power in each frequency bin averaged over the whole sweep, this effect was also responsible for the reduction in the frequency-domain amplitude observed in Figure 9.

The discrete nature of this flaw induction process naturally results in the cracks growing in discrete steps. Consequently, differences in the initial conditions of the samples, or in their fatigue histories, gives rise to a "quantization error" in the final crack dimensions (note the $\sim$ 6% difference, in Figure 8, between successive frequency points during the final damage increment). Nevertheless, we note that it is possible to mitigate this by using shorter sweeps when the crack approaches its target dimensions, or by using a phase-lock loop to track the resonance continuously.

Worthy of note is sample RD122, which exhibited a higher amplitude than the remaining samples for the first increment of the shift. This can be readily observed in Figure 8 as a steeper initial gradient. In spite of this, it followed the same general trend for the remainder of the exposure process, and the final crack length was within $\sim$ 8.5% of that of RD123 (Table 2). This suggests that Δf is indeed a more important measure of crack dimensions than amplitude history, but further corroboration with a larger sample set is required.

The NLR results displayed in Figure 11 confirmed the presence of contact flaws in all but the as-built samples, with the frequency drift showing a high sensitivity to smaller flaws and Nonlinear Metric 2 showing a sensitivity to larger flaws. Using a combination of various measures of nonlinearity enabled the surveying of the entire crack size range of the samples.

The optical micrographs shown in Figure 13 show the tortuous morphology of the cracks (albeit less tortuous than the ductile-torn side surface of RD120 in Figure 12), again consistent with an inter-granular fracture. Both Table 2 and Figure 16 demonstrate that a larger Δf corresponds to larger crack dimensions, with an approximately linear relationship, as shown by the trendline. In Figure 16, it is clear that there was a large increase in the crack lengths between the Δf steps, showing that finer increments can be applied to obtain a range of intermediate crack sizes. As expected, samples RD121 and RD123 had very similar crack dimensions, to within $\sim 0.02\%$ for the length. Finally, note that, despite the relatively coarse frequency shift increments of approximately 50 Hz, the crack in RD124 was very small and hardly surface-breaking (Figure 14). This indicates that any further work investigating finer damage increments must involve sectioning and SEM imaging of the samples to investigate internal crack morphology.

Future work should seek to corroborate these observations with a larger sample set to assess the statistical viability of the technique, as well as to determine a modelling-assisted quantitative relationship between Δf and crack dimensions. Future implementations of this technique using finer Δf increments will enable an evaluation of the sensitivity limits of various NDT techniques.

5. Conclusions

This paper presents a method for the rapid and controlled generation of mechanically fatigue-induced cracks in additively manufactured test coupons. The creation of these reference flaws is crucial for the certification of NDT techniques, which will enable the adoption of AM for critical applications.

To seed cracks in a controlled manner, a static tensile load is applied using steel bobs, whilst also exciting the system into a high-strain vibration mode. Utilizing resonance allows for the cracks to be seeded in a rapid, compact, and low-force setup. The bobs reduced the resonance frequency of the sample–bob assembly, increasing the strain at the tip of the notch, which acted as a stress raiser. Because this monitoring technique is non-invasive and utilizes the resonance of the entire sample–bob assembly, it does not require any probes in contact with the sample or near the vicinity of the crack, instead taking measurements with a laser Doppler vibrometer at an arbitrary location on the assembly. Through the judicious selection of the resonance mode shape and the location of stress-raising features, this technique provides much greater control over the crack location and morphology. Finally, this technique can be very quickly and inexpensively realized, taking a maximum of 15 min for the seeding of the largest crack in this study, and this timespan can be further reduced by increasing the excitation amplitude or the magnitude of the tensile load. The convenience of this technique makes it ideal for the creation of large sample sets, which can be used in statistically significant studies in both AM and NDT.

The experimental work shows the successful creation of five reference samples with seeded cracks of lengths between 0.27 and 5.6 mm and openings between 14 µm and 79 µm. The crack lengths are controlled using a continuous, no-contact measurement of the resonance frequency, allowing for the creation of very small flaws.

The cracks seeded in these samples were validated using Nonlinear Resonance and optical microscopy, with the former confirming the presence of cracking and the latter confirming the crack dimensions over the exposure process.

Author Contributions: Conceptualization, J.W. (James Watts); methodology, D.P., A.A. and J.W. (Jacques Wood); formal analysis, D.P.; investigation, A.A. and D.P.; resources, J.W. (Jacques Wood); data curation, A.A.; writing—original draft preparation, A.A. and D.P.; writing—review and editing, D.S. and J.W. (Julian Wright); visualization, D.P.; supervision, J.W. (James Watts); project administration, D.P. All authors have read and agreed to the published version of the manuscript.

Funding: This research received no external funding.

Data Availability Statement: Graph datasets are available online at https://doi.org/10.6084/m9.figshare.24050781.v1 (accessed on 20 October 2023).

Conflicts of Interest: The authors are affiliated with a company that offers non-destructive testing and declare that this work does not constitute any competing interests.

References

1. Blakey-Milner, B.; Gradl, P.; Snedden, G.; Brooks, M.; Pitot, J.; Lopez, E.; Leary, M.; Berto, F.; Du Plessis, A. Metal Additive Manufacturing in Aerospace: A Review. *Mater. Des.* **2021**, *209*, 110008. [CrossRef]
2. *ISO/ASTM TR 52906:2022*; Additive Manufacturing-Non-Destructive Testing-Intentionally Seeding Flaws in Metallic Parts. International Organization for Standardization: Geneva, Switzerland, 2022. Available online: https://www.iso.org/standard/75716.html (accessed on 20 October 2023).
3. Obaton, A.-F.; Butsch, B.; McDonough, S.; Carcreff, E.; Laroche, N.; Gaillard, Y.; Tarr, J.B.; Bouvet, P.; Cruz, R.; Donmez, A. Evaluation of Nondestructive Volumetric Testing Methods for Additively Manufactured Parts. In *Structural Integrity of Additive Manufactured Parts*; Shamsaei, N., Daniewicz, S., Hrabe, N., Beretta, S., Waller, J., Seifi, M., Eds.; ASTM International: West Conshohocken, PA, USA, 2020; pp. 51–91, ISBN 978-0-8031-7686-7.
4. Yanishevsky, M.; Martinez, M.; Mandache, C.; Khan, M.; Fahr, A.; Backman, D. Artificial Seeding of Fatigue Cracks in NDI Reference Coupons. *Insight Non-Destr. Test. Cond. Monit.* **2010**, *52*, 664–671. [CrossRef]
5. Yan, W.-T.; Holdsworth, S.; Kühn, I.; Mazza, E. Creep–Fatigue Crack Development from Short Crack Starters. *Mater. High Temp.* **2014**, *31*, 305–314. [CrossRef]
6. Richards, M.D.; Weeks, T.S.; McColskey, J.D.; Wang, B.; Wang, Y.-Y. Fatigue Pre-Cracking Curved Wide Plates in Bending. In Proceedings of the 2010 8th International Pipeline Conference, Calgary, AB, Canada, 27 September–1 October 2010; ASMEDC: Calgary, AB, Canada, 2010; Volume 4, pp. 237–244.
7. Kemppainen, M.; Virkkunen, I.; Pitkänen, J.; Paussu, R.; Hänninen, H. Advanced Flaw Production Method for In-Service Inspection Qualification Mock-Ups. *Nucl. Eng. Des.* **2003**, *224*, 105–117. [CrossRef]
8. Ekström, P.; Wåle, J. *Crack Characterisation for In-Service Inspection Planning*; Safety at Nucleur Power Plants; Swedish Radiation Safety Authority: Solna, Sweden, 1995; p. 32.
9. Preston, D.; Rodriguez Sanmartin, D.; Watts, J.; Wright, J. Controlled seeding of contact cracks in test pieces for the evaluation and validation of non-destructive testing systems. *F1000Research* **2023**, *12*, 1103. [CrossRef]
10. Non-Destructive Testing for Metal AM. Available online: https://thetandt.com/ (accessed on 30 October 2023).
11. 40-1000X USB Digital Microscope. Available online: https://caindahelp.com/40-1000x-usb-digital-microscope-p00092p1.html (accessed on 30 October 2023).
12. ImageJ. Available online: https://imagej.nih.gov/ (accessed on 30 October 2023).
13. Solodov, I.; Döring, D.; Busse, G. New Opportunities for NDT Using Non-Linear Interaction of Elastic Waves with Defects. *Stroj. Vestn. J. Mech. Eng.* **2018**, *57*, 169–182. [CrossRef]
14. Van Den Abeele, K.E.-A.; Sutin, A.; Carmeliet, J.; Johnson, P.A. Micro-Damage Diagnostics Using Nonlinear Elastic Wave Spectroscopy (NEWS). *NDT E Int.* **2001**, *34*, 239–248. [CrossRef]
15. Ashby, M.; Jones, D.R.H. Chapter 14: Micromechanisms of Fast Fracture. In *Engineering Materials 1: An Introduction to Their Properties and Applications*; Butterworth Heinemann: Oxford, UK, 1996; Volume 1, pp. 140–154.
16. Lynch, S.P.; Wanhill, R.J.H.; Byrnes, R.T.; Bray, G.H. Chapter 13—Fracture Toughness and Fracture Modes of Aerospace Aluminum–Lithium Alloys. In *Aluminum-Lithium Alloys*; Butterworth Heinemann: Oxford, UK, 2014; pp. 415–455.
17. Nenadic, N.G.; Wodenscheck, J.A.; Thurston, M.G.; Lewicki, D.G. Seeding Cracks Using a Fatigue Tester for Accelerated Gear Tooth Breaking. In *Rotating Machinery, Structural Health Monitoring, Shock and Vibration, Volume 5*; Conference Proceedings of the Society for Experimental Mechanics Series; Proulx, T., Ed.; Springer: New York, NY, USA, 2011; pp. 349–357, ISBN 978-1-4419-9427-1.
18. Murakami, Y.; Takagi, T.; Wada, K.; Matsunaga, H. Essential Structure of S-N Curve: Prediction of Fatigue Life and Fatigue Limit of Defective Materials and Nature of Scatter. *Int. J. Fatigue* **2021**, *146*, 106138. [CrossRef]

Disclaimer/Publisher's Note: The statements, opinions and data contained in all publications are solely those of the individual author(s) and contributor(s) and not of MDPI and/or the editor(s). MDPI and/or the editor(s) disclaim responsibility for any injury to people or property resulting from any ideas, methods, instructions or products referred to in the content.